Fe-zeolites for the adsorption and oxidative degradation of nitroaromatic compounds in water

Alina Gawel[1], Sarah Sühnholz[2,3], Anett Georgi[2], Frank-Dieter Kopinke[2], and Katrin Mackenzie[2]*

[1]Evonik Operations GmbH, Process Technology & Engineering, Paul-Baumann-Str. 1, D-45772 Marl, Germany

[2]Helmholtz-Center for Environmental Research - UFZ, Department of Environmental Engineering, Permoserstr. 15, D-04318 Leipzig, Germany

[3]Intrapore GmbH, Katernberger Str. 107, D-45327 Essen, Germany

Corresponding author

*Email: alina.gawel@evonik.com

KEYWORDS: nitroaromatic explosives; Trap-Ox Fe-zeolites; nanoremediation; ISCO; water treatment

Abstract

Nitroaromatic compounds (NACs) are prominent explosives. In this context, these toxic substances were released into the environment and cause long-lasting groundwater contamination. In preparation of a possible *in-situ* remediation, colloidal Fe-zeolites were investigated for their capabilities as adsorbents and oxidation catalysts. It was shown that the Fe-zeolites FeBEA35 and FeFAU55 are potent inorganic adsorbents for NACs and simultaneously capable of activating H_2O_2 as Fenton-like oxidation catalysts. Adsorption isotherms of 15 NACs on both zeolites were measured to evaluate the option of coupling adsorptive contaminant enrichment with oxidative degradation. The faujasite-type zeolite FeFAU55 showed a distinct S-type adsorption behaviour and reached significantly higher NAC loadings of > 20 wt%. For FeBEA35, L-type adsorption isotherms and maximum loadings q_{max} of about 4 wt% were obtained. Degradation of all NACs, monitored by nitrate formation, was observed. Apparent rate constants of the NACs with hydroxyl radicals in a homogeneous, stoichiometric Fenton reaction were related to the heterogeneous system to examine the role of adsorption on the oxidative degradation. Beneficial influence of the adsorption on the oxidation rates was identified. The results of this work open up promising prospects for future application of Fe-zeolites for the *in-situ* remediation of NAC-contaminated groundwater.

Environmental Implication

The target pollutants of this study are nitroaromatic compounds (NACs), i.e. 2,4,6-trinitrotoluene (TNT) and its derivatives. TNT itself as well as its natural degradation products, amino-nitrotoluenes, are proven to be both acutely and chronically toxic and carcinogenic. Worldwide, many thousands of sites where explosives were processed and handled are contaminated and in need of remediation to prevent further dispersal and discharge into, for example, potion water reservoirs. As an alternative to cost-intensive and lengthy pump-and-treat measures for the remediation of groundwater contaminated with NACs, we herein present Fe-zeolites as coupled adsorbents and oxidation catalysts for *in-situ* application.

1. Introduction

The nitroaromatic compound (NAC) 2,4,6-trinitrotoluene (TNT) is the most prominent explosive all over the world regarding armament, but also civilian use, e.g. for blasting in stone quarries.[1] Shipping, use, and disposal of this highly toxic explosive that is persistent in the environment has led to the contamination of many sites by TNT and its degradation and byproducts in former war zones, near blast sites, and armament factories. The U.S. Army estimates more than 1.2 million tons of soil contaminated with explosives on U.S. territory, and 3,240 sites in Germany alone are suspected of being contaminated with NACs.[2,3] Since for most NACs the range of acute and chronic adverse health effects on humans and animals is broad, including significant changes of the haemogram and mutagenic effects leading to high mortality of exposed individuals, remediation of contaminated sites is essential.[4,5]

Environmental contaminations with NACs are commonly treated by dredging and off-site disposal or treatment of the dredged soil coupled with either on-site clean-up of contaminated groundwater by pump-and-treat measures or monitored natural attenuation. However, natural attenuation proceeds slowly and is not a reliable remediation method if protective goods, like drinking water reservoirs or residential areas, are threatened by the contamination.[2,6] Especially for residual contaminations with a relatively low remaining pollutant load, nanoremediation-type measures which are based on *in-situ* generation of permeable reactive barriers (PRBs) offer an alternative to conventional lengthy pump-and-treat approaches.[7–9] Thereby, particle suspensions are injected into the aquifer to form an adsorptive and/or reactive zone after particle immobilization which is passed by the contaminated groundwater.[10,11] Adsorption barriers have the effect of retaining the contaminants within the treatment zone, allowing more time for natural attenuation without further spreading of the contaminant plume. For recalcitrant substances, however, pure adsorption barriers are often not sufficient; an additional pollutant degradation function is required.[12,13] Alternative methods for NAC removal exist, such as chemical reduction, e.g. with zero-valent iron, but this produces reduction products that have

comparable or even higher toxicities than the initial NAC contaminants.[14,15] However, some of the partially reduced NACs, like diaminonitrotoluenes (DANTs), are known to be removed from the aqueous phase due to reactions with soil organic matter.[16]

Chemical oxidation is known to be a powerful tool for NACs degradation and detoxification of contaminated water or soil. The application of various advanced oxidation processes (AOPs), like photocatalytic oxidation, ozonolysis, and Fenton-like reactions, for the treatment of NAC contaminations was previously described.[18–22] Compared to the parent compounds, oxidation products of NACs show significantly reduced toxicity, provided that a sufficient oxidation degree is achieved.[17] However, most AOPs for *in-situ* applications in aquifers or soils suffer from insufficient mixing of the reagents (oxidant and catalyst) with the contaminated compartments or clogging of flow paths by reaction products, e.g. iron oxides for applications of the Fenton reaction, or MnO_2 when MnO_4^- is used as oxidant.[23]

In order to effectively incorporate chemical oxidation into an *in-situ* PRB, Trap-Ox Fe-zeolites are the ideal material to accomplish that.[12] Colloidal properties and mobility of these particles in porous media such as aquifers were shown to be suitable for *in-situ* application.[11] Thus, it is envisaged that injection of a zeolite suspension followed by particle deposition and immobilization at the subsurface sediment leads to the formation of a permeable adsorption barrier in the aquifer. During groundwater passage through this barrier, contaminants are removed from the aqueous phase by adsorption. Zeolites are not only powerful adsorbents, but also - in contrast to carbon-based adsorbents - inert against strong oxidants. Fe-loaded zeolites are even active in hydrogen peroxide activation due to their content of isolated iron ions bound to the ion-exchange sites of the zeolite.[24,25] Therefore, in a second step, the loaded barrier is flushed with a diluted hydrogen peroxide solution before contaminant breakthrough. The deposition of the solid catalyst on the sediment, and thus the retention of the contamination in this zone, allows contact with the injected oxidant. This is equivalent to the effect of mixing of contaminated water and liquid injected oxidant, which otherwise cannot be achieved in an aquifer. Furthermore, in this way, also safety concerns known from conventional *in-situ* Fenton applications are avoided: using dissolved iron ions and oxidant solutions need a certain degree of mixing before or during injections, which causes gas and heat formation. In the Trap-Ox approach, H_2O_2 reacts with $Fe^{2+/3+}$ centers which are embedded into the zeolite structure and thus offers a much wider applicable pH range.[24] Compared to conventional *in-situ* Fenton oxidation, the need of low pH values (≤ 3) or organic complexing agents is eliminated. Consequently, Fe-zeolites are combined adsorbents and heterogeneous Fenton-like catalysts. They are able to de-couple OH• generation from quenching reactions within the aquifer matrix 'outside' the particles, such as natural organic matter (NOM). Reactive species are generated in the close proximity to the adsorbed target contaminants.[11,25] This decoupling should lead to a reduction of parasitic H_2O_2 consumption and avoids aquifer clogging by iron oxide precipitates.

Furthermore, as the PRB is regenerated by the oxidation of adsorbed contaminants, the cycle of continuous adsorption and periodic regeneration can be repeated multiple times.[12]

In this work, the general applicability of Trap-Ox Fe-zeolites for the adsorption and degradation of NACs is examined for the first time. Zeolites are available in a broad variety of framework types and compositions with different behaviour and properties. Two examples were chosen as Fe-zeolites, FeBEA35 and FeFAU55, and compared with regard to adsorption and mineralization of 15 NACs. These are common precursors, side- or transformation products of TNT found in the environment.[26] The two chosen zeolites represent the BEA and FAU framework type. They belong to the most important industrial zeolites with sufficiently large pore openings for accommodation of organic molecules (and specifically such with substituted aromatic rings) due to their 12 T-atom ring pores (T stands for Si or Al).[27]

2. Materials and methods

2.1 Materials

Trap-Ox Fe-zeolite FeBEA35 was supplied by Intrapore GmbH (Essen, Germany). FAU55/ZEOflair 200 was purchased from Zeochem (Rüti, Switzerland) and iron-loaded by liquid ion exchange using a method according to Gonzalez-Olmos *et al*.[12] FeBEA35 is a BEA-type zeolite with both straight, channel-shaped pores of 6.6 to 6.7 Å diameter and serpentine pores with a diameter of 5.6 to 5.7 Å. FeFAU55, in contrast, has pore openings with a 6.9 Å diameter with larger cavities of 11.9 Å, so-called supercages, at the inter-sections of the pores. A structural depiction of both zeolite types can be found in Figure SI-1. In Table 1, the properties of the two zeolite samples are summarized. Molar ratios of SiO_2 : Al_2O_3 (modulus) and Fe contents were determined by X-ray fluorescence analysis and BET specific surface areas by N_2 adsorption/desorption analysis as described in the supporting information of Qian *et al*.[28] Notably, the weight-normalized particle size distributions reveal significant fractions around 10 µm diameter (see Figure SI-3), different from the number-normalized values in Table 1.

Table 1: Properties of the Fe-zeolites studied in this work.

	FeBEA35	**FeFAU55**
Molar ratio of SiO_2 : Al_2O_3	35	55
Fe content [wt%]	1.3	0.4
BET surface area [m^2 g^{-1}]	627	765
Porosity [cm^3 g^{-1}]*	0.4	0.5
Pore limiting diameter [Å]*	6.7	7.4
Largest cavity diameter [Å]*	6.9	11.9

Particle diameter D_{10}, D_{50}, D_{90} [µm] (number-based)**	0.2, 0.3, 0.5	0.3, 0.5, 1.6

116 **according to the Database of Zeolite Structures[29] **see Figure SI-3*

117 The NACs examined in this work are listed in Table 2.

118 **Table 2: Abbreviations, suppliers, and purities of the NACs examined in this work.**

NAC	Abbreviation	Supplier	Purity
2,4,6-trinitrotoluene	TNT	AccuStandard	Certified reference quality
1,3,5-trinitrobenzene	TNB	AccuStandard	Certified reference quality
2,4-dinitrotoluene	2,4-DNT	Aldrich	97 %
2,6-dinitrotoluene	2,6-DNT	Alfa Aesar	97 %
1,3-dinitrobenzene	DNB	Sigma-Aldrich	Neat
2,4-dinitrobenzoic acid	DNBA	Aldrich	96 %
2-nitrotoluene	2-NT	Merck	Synthesis grade
4-nitrotoluene	4-NT	J&K	99 %
nitrobenzene	NB	Acros Organics	> 99 %
2-amino-4,6-dinitrotoluene	2-ADNT	Ceriliant	Analytical standard
4-amino-2,6-dinitrotoluene	4-ADNT	Ceriliant	Analytical standard
3,5-dinitroaniline	DNA	Aldrich	97 %
2,6-diamino-4-nitrotoluene	DA-4-NT	Aldrich	99 %
2,4-diamino-6-nitrotoluene	DA-6-NT	chemPUR	95 %
1,3-diamino-5-nitrobenzene	DANB	BLDpharm	> 95 %

119 Phenol (*p.a.*), H_2O_2 (30 %) and $FeSO_4 \cdot 7\ H_2O$ (*p.a.*) were purchased from Merck. Aniline (≥ 99.5 %)
120 was obtained from Sigma-Aldrich, oxalic acid dihydrate (98 %) from Alfa Aesar, KNO_3 (*puriss.*) and
121 HNO_3 (min. 65 %) from CHEMSOLUTE.

122 **2.2 Adsorption experiments**

123 Contaminant adsorption by the zeolite materials was studied according to a procedure previously
124 reported.[30] Briefly: for the measurement of the adsorption isotherms, various amounts of
125 FeBEA35 and FeFAU55 zeolites were added as aqueous suspensions to aqueous solutions of the
126 NACs as single components with concentrations in the range from 10 to 250 mg L^{-1}, resulting in

127 suspensions with 0.2 to 8 g L^{-1} solids and pH of 5 to 6. NACs concentrations were adjusted using
128 methanolic stock solutions ($c_{methanol}$ << 1 vol%). In this batch system, the equilibrium free NAC
129 concentrations $c_{free,NAC}$ covered the µm L^{-1} and mg L^{-1} range to cover the full Freundlich and
130 Langmuir isotherms and determine the maximum loading q_{max}. The suspensions were
131 equilibrated for at least 72 h by shaking to ensure that adsorptive equilibrium was reached in all
132 systems. The remaining freely dissolved NAC concentrations were measured with HPLC-DAD
133 (Shimadzu LC2020 system equipped with a Phenomenex Gemini 3 µm C_6-phenyl column) at a UV-
134 detector wavelength of 254 nm after filtration with 0.2 µm syringe filters (Whatman puradisc
135 PTFE). The isotherm data were evaluated according to the models of Freundlich and Langmuir
136 (see section SI-4).

137 **2.3 Oxidation experiments**

138 For the performance tests of the Trap-Ox system, 5 g L^{-1} zeolite suspensions in 10 mg L^{-1} aqueous
139 solutions of the single NACs were used (pH = 6). The system was ultra-sonicated for 15 min and
140 equilibrated overnight by stirring. In order to start the reaction, hydrogen peroxide was added to
141 reach a concentration of 3 wt%. H_2O_2 conversion was monitored. Nitrate formation was used to
142 follow the progress of pollutant oxidation because i) nitrate is a measure for deep oxidation of
143 the NAC and ii) nitrate is not adsorbed by the zeolite while NAC concentrations in the aqueous
144 phase are affected by adsorption equilibria. Nitrate concentration was determined by ion
145 chromatography (Dionex IC system equipped with an IonPac AS11-HC column) after filtration of
146 the samples with 0.2 µm syringe filters. Two independent experiments were conducted for each
147 NAC.

148 **2.4 Determination of apparent reaction-rate constants of NACs with OH•**

149 Apparent reaction-rate constants of the explosives with hydroxyl radicals were determined by
150 competition kinetics using a homogeneous, 'stoichiometric' Fenton reaction (pH_0 = 7) of 10 mg L^{-1}
151 NAC (corresponding to $c_{NAC,0}$ ≈ 40 – 80 µM) in the presence of 10 – 40 mg L^{-1} aniline or phenol as
152 competitor (corresponding to $c_{competitor,0}$ ≈ 100 µM). Aniline and phenol were used as competitor
153 agents because reliable reaction rate constants are available in the literature for those
154 compounds and they could be simultaneously analysed with the NACs using HPLC-DAD. Different
155 amounts of Fenton's reagent (molar ratio $n_{Fe(II)} : n_{H2O2}$ = 1 : 1, $c_{Fe(II)}$ = 100 – 400 µM) were added
156 subsequently to the aqueous solution of the two competing target compounds. The respective
157 amount of Fe(II) was dissolved first in the degassed solutions before adding H_2O_2 under vigorous
158 stirring. After 10 min reaction time, the reaction was quenched with methanol and the remaining
159 concentrations of NAC and aniline or phenol were measured with HPLC-DAD. From the ratio of
160 residual concentrations of NAC to aniline or phenol and the known second-order rate constants

for the reaction of aniline or phenol with OH• taken from literature, the respective apparent second-order rate constants of the explosives were calculated (see section SI-3).[31]

3. Results

3.1 Adsorption of NACs to Fe-zeolites

As Fe-zeolites are considered to create an *in-situ* adsorption barrier for contaminant retention before being regenerated by the Fenton-like reaction, it is crucial to know the adsorption parameters of the target contaminants to the zeolites. From those parameters, lifetime of the barrier before contaminant breakthrough and thus the optimal date for the regeneration step can be estimated.[10]

In Figure 1, the correlation between the loading q_i of the individual explosive *i* on the zeolite and its remaining freely dissolved concentration $c_{free,i}$ at equilibrium is shown exemplarily for 4-ADNT at the two studied zeolite types (all graphs shown in Figures SI-6 to 19).

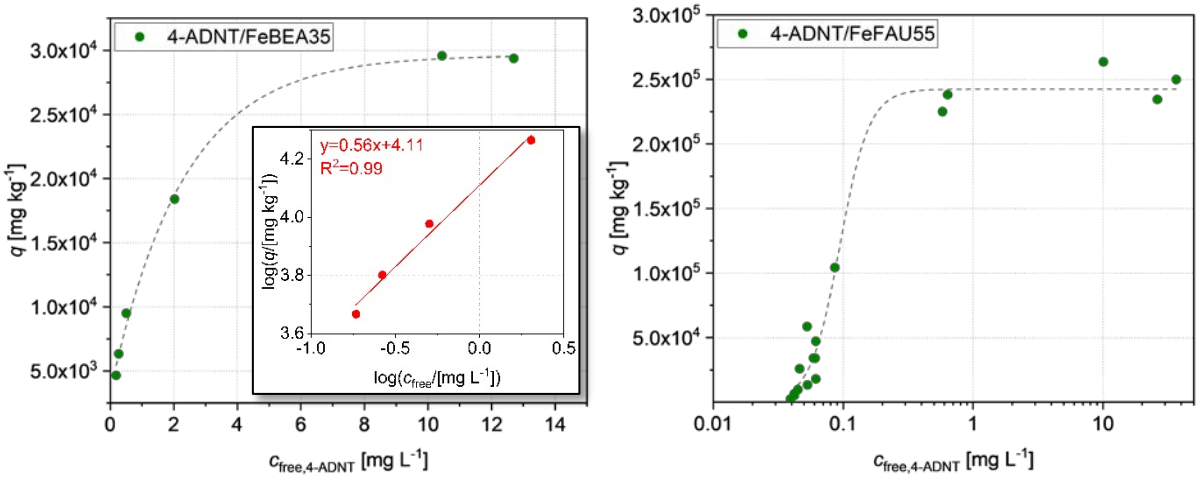

Figure 1: Adsorption isotherms of 4-ADNT on Fe-zeolites FeBEA35 (left, insert: Freundlich plot fitted to $c_{free,4\text{-}ADNT}$ < 2 mg L^{-1}) and FeFAU55 (right, with logarithmic x-axis). $c_{free,4\text{-}ADNT}$ = 0.039 – 37 mg L^{-1}, $c_{zeolite}$ = 0.06 – 4 g L^{-1}; values for high loadings on FeFAU55 (c_{free} > 0.6 mg L^{-1}) might be biased by solubility limitations[32].

The example of 4-ADNT represents the qualitative shape of the adsorption isotherms of most of the other examined NACs and shows that the adsorption mechanisms at the two types of zeolites are different. For FeBEA35, L-type isotherms are obtained.[33] In gas-phase adsorption, this isotherm shape is typical for the monolayer adsorption of small organic molecules from the water phase to micro- and mesoporous materials. In case of L-type isotherms, sorption affinity (expressed as single-point sorption coefficient K_D) decreases with growing contaminant loading

184 q at the surface of the microporous adsorbent which leads to a monotonic function (Figure 2,
185 left).

186 However, adsorption on FeFAU55 can rather be described by a S-type isotherm, which is why we
187 chose a logarithmic x-axis for the graphical representation. In gas phase adsorption, this isotherm
188 shape occurs in cases where the presence of an adsorbed monolayer strongly enhances the
189 adsorption of additional molecules, a phenomenon which might also occur during adsorption of
190 NACs in the supercages of FeFAU55 from the liquid phase. S-type isotherms were previously
191 observed for the adsorption of aromatic compounds to faujasite, e.g. trichlorophenol, and
192 attributed to intermolecular interactions inside the supercages of this zeolite type.[34] S-type
193 isotherms reach a maximum K_D at a certain loading q (in case of the example 4-ADNT at
194 $K_D \approx 1.4 \cdot 10^6$ L kg^{-1}), which afterwards decreases again (Figure 2, right). Graphs for all NACs are
195 given in Figures SI-6 to 19. This observation might be linked to the structure of FeFAU55, whereby
196 the adsorbent loading reaches a maximum q_{max} ≈ 25 wt% after complete pore filling of the
197 supercages. Note that the maximum adsorption coefficients K_D are much higher on FeFAU55
198 compared to FeBEA35.

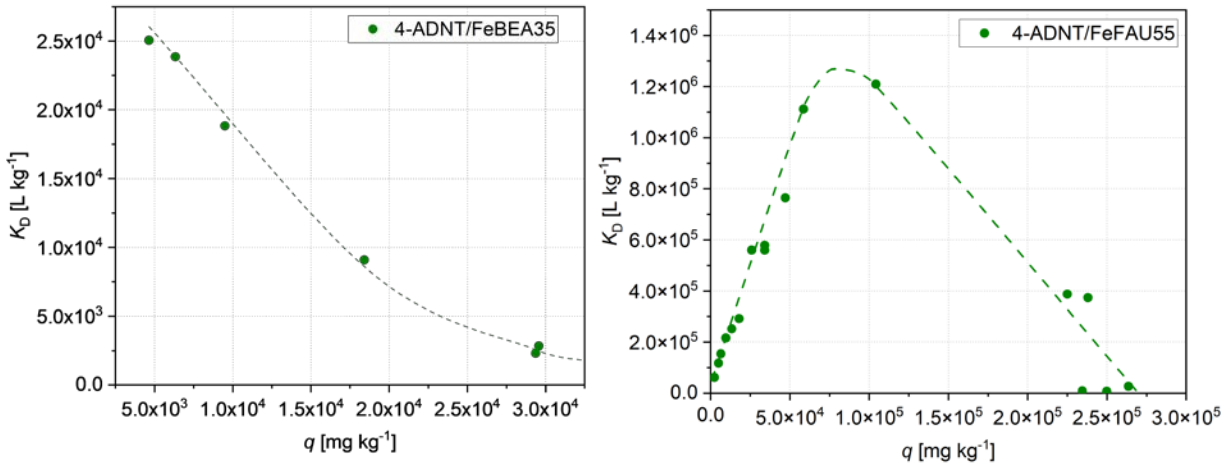

199

200 **Figure 2: Sorption coefficients K_D of 4-ADNT versus the loading q for the adsorption to**
201 **FeBEA35 (left) and FeFAU55 (right); $c_{free,4\text{-}ADNT}$ = 0.039 - 37 mg L^{-1}, $c_{zeolite}$ = 0.06 – 4 g L^{-1}. Dashed**
202 **lines are provided to guide the eye.**

203 In order to provide a basis for comparison of the adsorption behaviour of the various NACs to the
204 chosen Fe-zeolites, adsorption isotherms were measured and evaluated using the most common
205 models (Freundlich and Langmuir). In Table 3, the resulting Freundlich parameters logK_F and n
206 and the fitted concentration range for each NAC are given. They can be used to estimate
207 breakthrough times through an adsorbent-loaded column or permeable adsorption zone under
208 certain conditions.[10] Table 4 summarizes the associated values for maximum loading q_{max} and, if
209 applicable, maximum K_D values (for NAC adsorption on FeFAU55). The full set of adsorption data
210 received from adsorption experiments using the two Fe-zeolites and all NACs (except for DNBA)

included into this study are depicted in Figures SI-6 to 19. S-type isotherms were split into the nearly linear range for Freundlich evaluation at low q and the Langmuir range when approaching saturation at high q. Thereby, the values constituting the rising branch of the K_D vs. q plot were assigned to the Freundlich isotherm and the falling branch to the Langmuir isotherm, respectively. Adsorption of DNBA in its anionic form ($pK_A \approx 1.4$[35]) to both zeolites was also tested, but the depletion in the aqueous phase concentration due to adsorption was too low even at high adsorbent dosages for the derivation of reliable adsorption isotherms. Under the given conditions, K_D values in the range of only 10 L kg^{-1} were obtained for this substance. This can be attributed to the ionic character, i.e. significantly higher hydrophilicity, and repellent electrostatic interactions between zeolite surfaces and the DNBA anion.

Table 3: Adsorption isotherm parameters of NACs on Fe-zeolites FeBEA35 and FeFAU55 according to Freundlich equation ($c_{total,NAC}$ = 10 – 250 mg L^{-1}, $c_{zeolite}$ = 0.02 – 8 g L^{-1}).

	FeBEA35			FeFAU55		
	$\log\frac{K_F}{[mg^{1-n} \cdot L^n \cdot kg^{-1}]}$	n [-]	NAC conc. range used for fitting $c_{free,NAC}$ [mg L^{-1}]	$\log\frac{K_F}{[mg^{1-n} \cdot L^n \cdot kg^{-1}]}$	n [-]	NAC conc. range used for fitting $c_{free,NAC}$ [mg L^{-1}]
TNT	4.1	0.63	≤ 0.6	13.1	6	≤ 0.1
TNB	3.4	0.55	≤ 8.2	4.5	1.4	≤ 1.6
2,4-DNT	4.6	0.72	≤ 0.3	8.8	9.1	≤ 0.4
2,6-DNT	4.3	0.73	≤ 0.8	21.3	13.9	≤ 0.1
DNB	3.8	0.78	≤ 2.9	4.8	9.0	≤ 0.9
2-ADNT	4.2	0.41	≤ 1.5	5.9	2.9	≤ 0.6
4-ADNT	4.1	0.56	≤ 2.0	10.4	4.8	≤ 0.1
DNA	3.7	0.62	≤ 2.9	4.7	2.4	≤ 1.8
2-NT	3.8	0.71	≤ 2.3	8.7	16.8	≤ 0.6
4-NT	4.4	0.55	≤ 0.6	7.0	5.1	≤ 0.4
NB	3.7	0.88	≤ 2.0	1.6	28.9	≤ 1.3
DA-4-NT	4.3	0.45	≤ 2.0	3.5	0.91	≤ 66
DA-6-NT	4.4	0.62	≤ 0.3	3.9	0.88	≤ 33
DANB	3.9	0.76	≤ 1.8	3.1	1.1	≤ 73

The data shown in Table 3 are calculated based on the decrease in aqueous phase (i.e. freely dissolved) concentrations due to adsorption. Freundlich parameters are valid for the

concentration ranges given for each NAC. The resulting Freundlich parameters for sorption of NACs on/in zeolite FeFAU55 appear 'abnormally' (e.g. $n >> 1$), because the Freundlich model was not developed for S-type isotherms. Nevertheless, due to its empirical nature it may be formally applied and the resulting parameters can be used for modelling of breakthrough profiles. In case of DA-6-NT adsorption is superimposed by a partial chemical transformation of the substance induced by the presence of the zeolites. Without any additional reagent, a second peak with lower retention than DA-6-NT and absorption maxima at λ = 212 and 236 nm appeared in the HPLC chromatograms. This observation was accompanied by a slowly progressing dark discolouration of the samples. The by-product was not identified, but DA-6-NT is therefore excluded from further comparisons. It was frequently reported in the literature that aromatic amines undergo reactions with clay minerals, leading to formation of covalent bonds to the minerals or oligomerization.[36–38] It is conceivable that DA-6-NT is also prone to such reactions with the zeolite surface and it cannot be excluded that other, particularly amino-NACs show similar behaviour, although not accompanied by visible discolouration. Here, spectroscopical characterization of the loaded zeolites could provide further insight.

Table 4: Experimental maximum loadings $q_{max,exp}$ of NACs on Fe-zeolites FeBEA35 and FeFAU55 and calculated maximum loadings q_{max} according to the Langmuir equation. For S-type adsorption isotherms, also the maximum sorption coefficients $K_{D,max}$ and the respective loadings are given ($c_{total,NAC}$ = 10 – 250 mg L^{-1}, $c_{zeolite}$ = 0.02 – 8 g L^{-1}). For the adsorption of DA-4-NT, DA-6-NT, and DANB to FeFAU55, no $K_{D,max}$ values could be determined due to L-type isotherm behaviour.

	FeBEA35			FeFAU55			
	$q_{max,exp}$ [wt%]	q_{max} [wt%]	q_{max} [mol kg^{-1}]	$q_{max,exp}$ [wt%]	$K_{D,max}$ [10^5 L kg^{-1}] (at q [mol kg^{-1}])	q_{max} [wt%]	q_{max} [mol kg^{-1}]
TNT	2.3	2.3	0.10	15.7	13.3 (0.24)	22.6	0.99
TNB	1.1	1.6	0.07	16.2	0.7 (0.25)	28.0	1.31
2,4-DNT	3.6	5.1	0.28	24.1	3.9 (0.29)	24.3	1.34
2,6-DNT	4.0	3.8	0.21	20.1	12.6 (0.29)	22.9	1.26
DNB	3.5	3.7	0.22	24.4	0.8 (0.32)	25.6	1.52
2-ADNT	3.6	3.8	0.19	25.1	2.8 (0.27)	22.3	1.13
4-ADNT	3.0	3.2	0.16	26.4	13.8 (0.27)	24.5	1.24
DNA	2.1	1.8	0.10	23.6	1.1 (0.29)	24.0	1.31
2-NT	3.6	3.7	0.27	17.8	1.4 (0.39)	21.4	1.56
4-NT	5.0	5.3	0.39	25.4	3.2 (0.39)	23.4	1.70

NB	3.8	3.6	0.29	18.7	0.8 (0.43)	19.2	1.56
DA-4-NT	5.1	5.1	0.30	16.4	n.a.	15.7	0.94
DA-6-NT	25.6*	15.6*	0.93*	27.2	n.a.	32.3	1.93
DANB	3.8	3.1	0.20	22.0	n.a.	21.6	1.41

* Adsorption of DA-6-NT is superimposed by chemical transformations giving rise to overestimation of q_{max}.

Maximum loadings of the NACs on FeBEA35 range from 1.6 wt% (TNB) to 5.3 wt% (4-NT), whereas FeFAU55 maximum loadings between 15.7 wt% (DA-4-NT) to 28.0 wt% (TNB) were found. An exception, as mentioned above, is DA-6-NT with a formally calculated q_{max} of 15.6 wt% on FeBEA35 and 32.3 wt% on FeFAU55, respectively. The values derived for the adsorption of DANB on FeFAU55 should also be considered with caution due to the relatively large error range (Figure SI-17). In case of FeBEA35, the highest loadings could be achieved with 4-NT and DA-4-NT, the lowest with TNB and TNT. For FeFAU55, also 4-NT reached the highest loading, followed by 2-NT and NB. Lowest loadings were achieved for DA-4-NT and TNT. Compared to other adsorbents from the literature, the obtained maximum loadings for FeFAU55 are high and in the range of highly specialized adsorbents, like covalent organic frameworks, while loadings similar to those reached with FeBEA35 were also reported for minerals such as montmorillonite or hectorite (Table SI-5).[39–41] When calculating q_{max} on a molar basis, the deviations of q_{max} between the different NACs are smaller, with (0.21 ± 0.09) mol kg^{-1} for FeBEA35 and (1.33 ± 0.22) mol kg^{-1} for FeFAU55 (DA-6-NT excluded). On the molar basis, adsorption mechanisms of the various NACs seem to be specific for each zeolite. The interaction between NACs as electron-deficient π-acceptors and surfaces with negative charge, e.g. phyllosilicates or basal siloxane surfaces, is already described in the literature.[42,43] Due to the strong negative charge of the zeolites' inner surfaces caused by the incorporation of Al^{3+} in the silicate framework, those literature findings can likely be transferred to the Trap-Ox Fe-zeolites.[44] The n-π electron donor-acceptor (EDA) interactions of surface oxygen with NACs were reported to lead to adsorption that was far more pronounced (5 orders of magnitude higher) than expectable based on octanol-water partition coefficients (K_{OW} values), representing hydrophobic interactions.[42,45] Also Haderlein *et al.* showed that there is no correlation between K_D and K_{OW} for NACs adsorption to clay minerals, leading to the assumption that hydrophobic interactions are not the main driver of adsorption.[40,46] FTIR measurements confirmed the theory of n-π EDA complex formation by proving a coplanar orientation of NACs towards the siloxane surface.[40–43,45–47] However, the values of q_{max} on FeFAU55 are remarkably high. Furthermore, Freundlich isotherms of the adsorption to FeFAU55 are extremely steep, resulting in values for $n > 1$, indicating that adsorption of a monolayer favours adsorption of further molecules. Those observations lead to the conclusion that the

277 adsorption of NACs to FeFAU55 proceeds via π-π stacking of molecules adsorbed within the 3D-
278 supercages of FeFAU55 with diameters of 11.9 Å sterically allowing pore filling. This stacking of
279 NACs is hardly possible in the channel-shaped pores of FeBEA35 as the molecules can only enter
280 the pores in a queue.

281 Comparing the different substance classes for their adsorption to FeFAU55, it is obvious that
282 $K_{D,max}$ values are consistently higher for nitrotoluenes than for the respective nitrobenzenes. This
283 observation is in contrast with the findings of Haderlein *et al.*, who reported decreased K_D values
284 for the adsorption of *ortho*- and *para*-methyl NACs to clay minerals. In case of *ortho*-substituted
285 compounds, the authors attribute this effect to the steric hindrance of the coplanar orientation,
286 the so-called *ortho*-effect.[40] The pores of zeolites, however, offer different steric conditions and
287 seem to enable specific adsorptive interactions. Extremely high $K_{D,max}$ values > 10^6 L kg^{-1},
288 especially TNT, 2,6-DNT, and 4-ADNT, i.e. NACs with two nitro groups in ortho-position to the
289 methyl group, catch the eye. It was previously reported that ortho nitro groups are forced out of
290 the ring plane.[48]

291 A more detailed inspection of $K_{D,max}$-values in Table 4 for adsorption on FeFAU55 reveals a
292 remarkable correlation: the number of nitro groups in the adsorbate molecule which are twisted
293 out of the aromatic plane (i.e. in ortho-position to another substituent) correlates positively with
294 their adsorption affinity. This effect is obvious for the DNT isomers and for the ADNT isomers (see
295 Table 4 and Figure SI-25). Hence, these nitro groups seem to play a key role for adsorption in
296 FeFAU55. How to interpret the steric effect, planar vs. out-of-plane twisted nitro groups? One
297 can assume that planar nitro groups have a better chance to delocalize the partial positive charge
298 at the nitrogen atom across the aromatic π-electron system, whereas aplanar nitro groups have
299 a more localized positively charged N-atom. If such positively charged atoms are beneficial for
300 interactions with negatively charged sites at the zeolite surface, then it is plausible that the
301 stereochemistry of the nitro groups affects significantly or even dominantly adsorption of the
302 aromatic molecules.

303 It is noteworthy that NACs with two amino groups (DA-4-NT, DA-6-NT, and DANB) nevertheless
304 differ in their adsorption behaviour on FeFAU55 compared to the other NACs, despite
305 comparably high loadings. Similarities in their adsorption behaviour to FeBEA35 can be seen with
306 Freundlich exponents close to 1 and no maximum K_D (Table 3). Figure 3 shows the plot of K_D
307 versus q for DANB as an example of how K_D is influenced by already adsorbed contaminant layers.
308 All plots are shown in Figure SI-6 to 19.

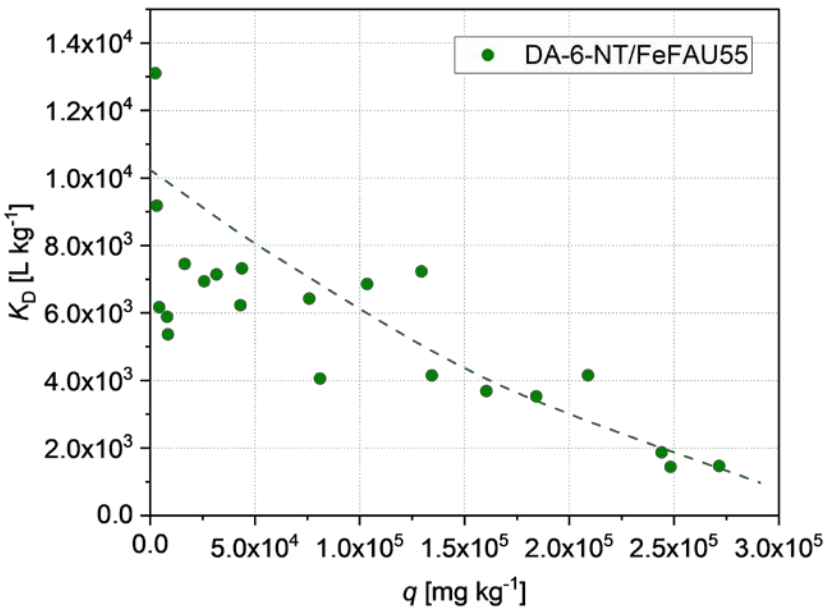

Figure 3: Impact of loading *q* on the sorption coefficient K_D as measure for adsorption affinity in the adsorption of DA-6-NT to FeFAU55 ($c_{free,DA\text{-}6\text{-}NT}$ = 0.2 – 185 mg L^{-1}, $c_{zeolite}$ = 0.25 – 4 g L^{-1}, dashed line provided to guide the eye).

This observation indicates that diamino-nitroaromatics do not reach pore filling after adsorption to FeFAU55 like the other NACs. It is likely that their interaction with the zeolite proceeds partially via the formation of hydrogen bonds between the amine hydrogen and electron pairs of surface oxygen, leading to a non-co-planar orientation of the adsorbed molecules on the surface and similar adsorption parameters as observed on FeBEA35.[49] In future studies, spectral analysis of the loaded zeolites could yield further insight into the adsorption mechanism of NACs to Fe-exchanged zeolites.

3.2 Oxidation of NACs

During *in-situ* application, a PRB from Trap-Ox zeolites needs to be regenerated with H_2O_2 to oxidize the adsorbed contaminants and restore adsorption capacity of the barrier after the adsorption phase. To assess their degradability in the Trap-Ox system, NACs adsorbed to the two zeolites under investigation were therefore oxidized by the addition of H_2O_2 to the suspension. With total NAC concentrations of 10 mg L^{-1} and a zeolite concentration of 5 g L^{-1}, an experimental setup was chosen where the major amount of the NACs is present in the adsorbed state (q_0 ≈ 0.2 wt%, c_{free} << 1 mg L^{-1}, compare Figures SI-6 to 19). Due to the large extent of adsorption of the NACs, educt depletion cannot be directly measured by analysis of the liquid phase. As a plausible indicator for progressing NAC oxidation, the formation of nitrate during the reaction was utilized. In Figure 4, the nitrate yields, normalized to the maximal possible elimination of nitro groups at full oxidation, are shown. Thereby, it is assumed that nitrogen from amino groups

332 is not converted to nitrate, which is in accordance with the obtained nitrate yields. It was
333 reported that during the Fenton-like oxidation of aniline, the amino group is converted to
334 ammonium.[50]

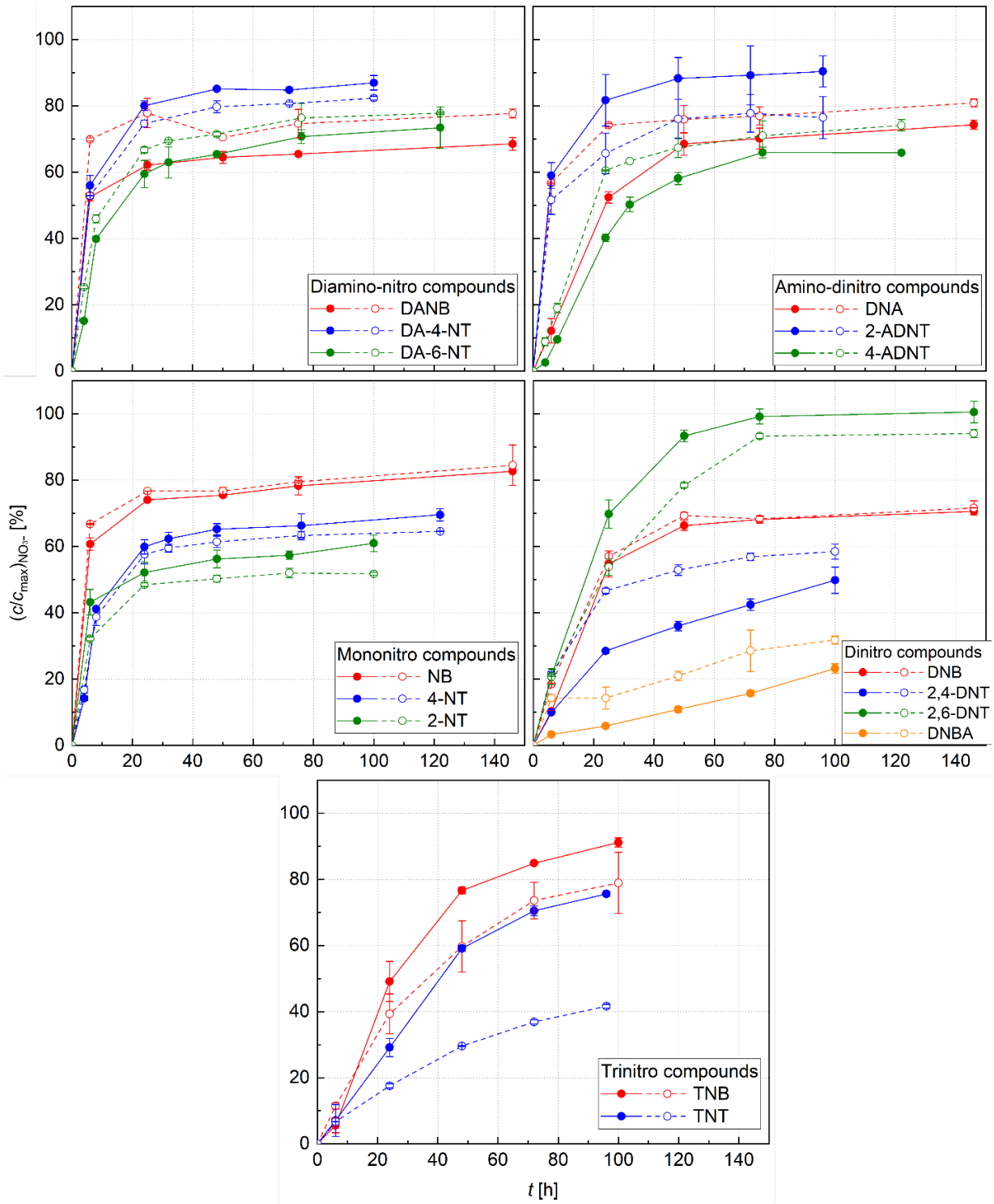

Figure 4: Nitrate yields in the Fenton-like oxidation of NACs with FeBEA35 (solid symbols/lines) and FeFAU55 (empty symbols/dashed lines). Nitro- and aminobenzenes are depicted in red, NACs with a *para*-nitro group in blue, and without a *para*-nitro group in green ($c_{NAC,0}$ = 10 mg L^{-1}, $c_{zeolite}$ = 5 g L^{-1}, $c_{H2O2,0}$ = 3 wt%). Error bars represent the deviation of single values from the mean of two independent experiments.

It is noticeable that the nitrate yields for all NACs except for 2,6-DNT do not approach 100 % during the observation period of 100 h, although a plateau in nitrate formation is reached or emerges (Figure 4) and the H_2O_2 concentration in the system is still on average 70 % of the initial value at that time (Figure SI-22).

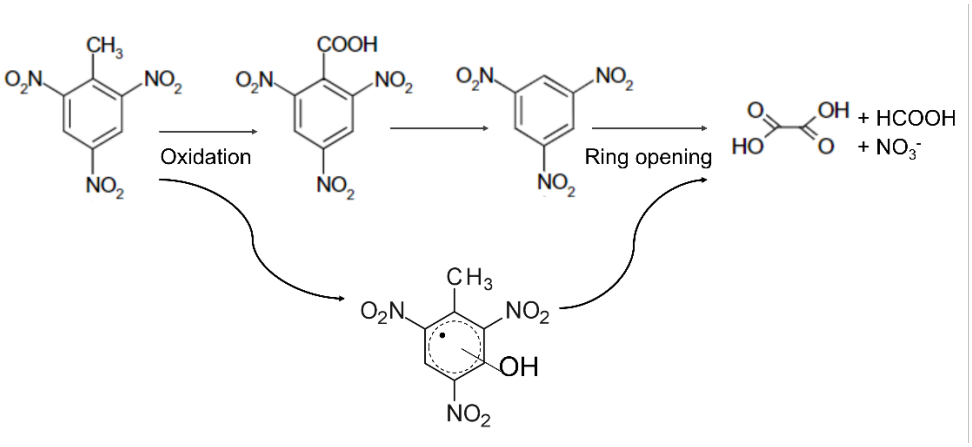

Figure 5: Suspected oxidation mechanism of TNT in Fenton-like oxidation systems based on Liou *et al.*[51]

Several authors describe the hydroxyl-radical driven oxidation of NACs as mainly proceeding via (i) the oxidation of the methyl group forming aldehydes and benzoic acids and (ii) hydroxylation of the aromatic ring and finally ring opening (Figure 5). This mechanism is also likely for the heterogeneous Fenton system, as we could identify partial desorption of trinitrobenzoic acid and TNB from FeBEA35 after addition of H_2O_2 to a sample treated with Trap-Ox (see section SI-7). As final degradation products, Fenton-like oxidation is reported to yield mainly short-chain carboxylic acids and nitrate.[48,52–55] Thereby, also gaps in the nitrogen balances or discrepancies between nitrate formation and degradation rates of NACs were reported. Ho *et al.* and Grätzel *et al.* proposed nitromuconic acid derivatives as nitrated aliphatic intermediates in photooxidation of NACs.[54,56] Similarly, García Einschlag *et al.* reported the formation of unidentified nitrated intermediates during UV/H_2O_2 treatment of various NACs. Tanaka *et al.* found also ammonium as a reduction product of the photocatalytic degradation of nitrophenols using TiO_2 as catalyst.[53,55] Nevertheless, repeated nitrate measurements of some samples after the depicted reaction time indicate slowly ongoing nitrate formation (section SI-5). Therefore, relocation of the reaction from the adsorbed to the dissolved state for ring-opened, more hydrophilic reaction intermediates, leading to lower degradation rates in the Trap-Ox system, can be postulated. The slow nitrate release from DNBA as a substance that is only slightly adsorbed (less than 10 % under the given conditions) supports this assumption. It should be noted that excessive production of short-chain carboxylic acids, such as oxalic acid, as degradation product could decrease the catalytic performance of Trap-Ox Fe-zeolites due to complexation of the embedded iron (see section SI-2) and should be investigated more deeply,

as well as options to re-load the zeolites with Fe *in-situ*. Furthermore, Oh *et al.* suspected the formation of additional nitrogen species, such as N_2O or NO_2^-, when retrieving only 92.2 % of nitrogen in form of NO_3^- and NH_4^+ after sequential treatment of TNT with Fe^0 and Fenton oxidation.[57] Another possible explanation for the gap in the nitrogen balance is the blockage of certain areas of the zeolite pores by unoxidized, adsorbed NAC which leads to a slow-down of the oxidation.

From the measured nitrate concentrations resulting from the oxidation, first-order rate constants for the heterogeneous reaction ($k_{\mathrm{het,FeBEA35}}$ and $k_{\mathrm{het,FeFAU55}}$) were determined. For this purpose, measured values at low conversion levels (< 50 %) were used to minimize the impact of secondary reactions. The k_{het}-values are given in Table 5. In the heterogeneous system, the reaction constants obtained vary over three orders of magnitude. With 0.003 h^{-1} for FeBEA35 and 0.005 h^{-1} for FeFAU55, respectively, by far the lowest constants were obtained for DNBA, which is the only anionic substance under investigation. All the other tri- and dinitro compounds yield rate constants between 0.01 and 0.1 h^{-1} with the sequence TNB < TNT < DNTs < DNB.

Whereas nitrate release from both dinitrotoluene isomers is similar using FeBEA35 (k_{het} = 0.04 h^{-1} for 2,4-DNT and 0.05 h^{-1} for 2,6-DNT), a more pronounced difference is obvious using FeFAU55 (0.07 h^{-1} for 2,4-DNT and 0.03 h^{-1} for 2,6-DNT). With regard to the sorption characteristics of the DNTs on FeFAU55, it is striking in this context that 2,4-DNT exhibits significantly higher Freundlich parameters and $K_{\mathrm{D,max}}$ values than 2,6-DNT (12.6 vs. 3.9 · 10^5 L kg^{-1} both at a loading of 0.29 mol kg^{-1}). At the same time, maximum loading of 2,4-DNT is higher (1.34 vs. 1.26 mol kg^{-1}).

Regarding the amino-dinitro compounds, it is noticeable that the nitrate release from 2-ADNT (k_{het} = 0.2 h^{-1} on both zeolites) is significantly faster than from 4-ADNT ($k_{\mathrm{het,FeBEA35}}$ = 0.04 h^{-1} and $k_{\mathrm{het,FeFAU55}}$ = 0.07 h^{-1}). 4-ADNT is again a NAC with an extremely high $K_{\mathrm{D,max}}$ value at FeFAU55 (13.8 compared to 2.8 · 10^5 L kg^{-1} both at a loading of 0.27 mol kg^{-1}). There is one more NAC with a $K_{\mathrm{D,max}}$ value in a comparable range like 2,6-DNT and 4-ADNT that simultaneously shows a low rate constant of only 0.01 h^{-1} on FeFAU55: TNT reaches a $K_{\mathrm{D,max}}$ value of 13.3 · 10^5 L kg^{-1} at a loading of 0.24 mol kg^{-1} and at the same time the lowest q_{max} of all NACs with 0.99 mol kg^{-1}. On the other hand, nitrate formation from DNA is considerably faster using FeFAU55 than FeBEA35 ($k_{\mathrm{het,FeFAU55}}$ = 0.2 h^{-1} compared to $k_{\mathrm{het,FeBEA35}}$ = 0.05 h^{-1}). With 1.1 · 10^5 L kg^{-1}, this substance reaches a comparably low $K_{\mathrm{D,max}}$ value. A particularly high sorption affinity (in the form of a high $K_{\mathrm{D,max}}$ value) is clearly disadvantageous for the oxidative degradation of the NACs. Here, it is possible that the strong and specific adsorptive interactions, which occurs predominantly for NACs with non-coplanar nitro groups in *ortho*-methyl position, stabilize or shield the NAC against radical attack. The other NACs (mononitro and diaminonitro compounds) show rate constants between 0.1 and 0.4 h^{-1} with the sequence 4-NT ≈ DA-6-NT < 2-NT ≈ DA-4-NT < NB < DANB. The fact that nitrobenzenes show a faster nitrate release compared to nitrotoluenes can be attributed to the

405 different reaction mechanism, since the attack on the methyl group as the often described first
406 reaction step is omitted in nitrobenzenes.

407 **Table 5: First-order reaction rate constants of NAC degradation in the heterogeneous, Fenton-**
408 **like Trap-Ox system k_{het} using FeBEA35 and FeFAU55 as adsorbents and catalysts**
409 **($c_{total,NAC,0}$ = 10 mg L^{-1}, $c_{zeolite}$ = 5 g L^{-1}, $c_{H2O2,0}$ = 3 wt%) and the respective apparent second-order**
410 **rate constants $k_{OH\cdot,app}$ of the homogeneous, stoichiometric Fenton reaction (averaged from**
411 **competition kinetics with aniline or phenol; $c_{NAC,0}$ ≈ 40 - 80 µM, $c_{aniline/phenol,0}$ = 100 µM,**
412 **$c_{total,H2O2/Fe(II)}$ = 100 – 400 µM; for more details see section SI-3).**

NAC	$k_{het,FeBEA35}$ [h^{-1}]	$k_{het,FeFAU55}$ [h^{-1}]	$k_{OH\cdot,app}$ [10^9 L mol^{-1} s^{-1}]
TNT	0.017	0.01	1.02
TNB	0.041	0.023	0.165
2,4-DNT	0.036	0.067	2.6
2,6-DNT	0.047	0.034	2
DNB	0.058	0.063	0.5
DNBA [1)]	0.0025	0.0054	0.3
2-ADNT	0.18	0.2	16
4-ADNT	0.037	0.066	6.3
DNA	0.048	0.2	14
2-NT	0.2	0.18	13.4
4-NT	0.1	0.1	13
NB	0.2	0.25	7
DA-4-NT	0.18	0.18	20
DA-6-NT	0.1	0.1	32
DANB	0.25	0.4	31

413 [1)] as anion (pK_a = 1.4)[35]

414 The dominant reactive species in the Fenton reaction and also in the Trap-Ox process are hydroxyl
415 radicals. To assess possible influences of the adsorption on the selectivity of the Fenton-like
416 reactions, second-order rate constants of the various NACs with OH-radicals were measured in a
417 homogeneous Fenton reaction for comparison. They can be used to estimate the reactivity of the
418 freely dissolved compounds. OH-attack is the first step but not the only relevant factor for
419 mineralization and nitrate release which was measured in the heterogeneous systems. A
420 common method to determine second-order reaction rate constants, e.g. with hydroxyl radicals
421 in a Fenton-like approach, is to follow the direct competitive reaction kinetics of a target and a
422 reference compound with known rate constant. In fact, the determination of true second-order
423 rate constants from competition experiments relies on certain pre-conditions which are further
424 discussed in section SI-3. As this is difficult to verify for all considered compounds, we address
425 the experimentally determined values as apparent rate constants $k_{OH\cdot,app}$. Nevertheless, they
426 provide relevant information on the ease of oxidation of the various NACs in Fenton-like systems

427 where OH• are considered as main oxidant species. $k_{OH\cdot,app}$ values, averaged from those derived
428 from competitive reaction with phenol and aniline, are given in Table 5. The full dataset is given
429 in section SI-3.

430 The apparent second-order rate constants for the homogeneous Fenton reaction of the studied
431 NACs vary over three orders of magnitude. It should be noted that rate constants $k_{OH\cdot,app} > 10 \cdot$
432 10^9 L mol^{-1} s^{-1} approach the diffusion-controlled limit of the reaction in water. One can speculate
433 that the rate-determining primary step may change (other radicals in addition to OH• may
434 contribute) and variations of those apparent rate constants should be interpreted with due
435 caution. Furthermore, for some NACs, the double-logarithmic plots from which the values for
436 $k_{OH\cdot,app}$ were derived (shown in Figure SI-4) are not strictly linear (e.g. in case of DNB) or forced
437 regression through the zero point (e.g. for TNB). Nevertheless, it is useful to know a gradation of
438 reactivities of the NACs in mixtures expected to occur in the field in order to be able to adjust
439 reaction conditions and stoichiometries to the targeted problem substances.

440 The obtained $k_{OH\cdot,app}$ values increase in the order TNB ≈ DNBA < DNB < TNT < 2,6-DNT < 2,4-DNT
441 < 4-ADNT < NB < 4-NT ≈ 2-NT < DNA < 2-ADNT < DA-4-NT < DANB ≈ DA-6-NT. It becomes obvious
442 that $k_{OH\cdot,app}$ increases with increasing number of amino groups in the molecule and decreases
443 with increasing number of nitro groups. Since nitro groups exert an electron-withdrawing effect
444 on the aromatic ring system and thus reduce the electron density, substrate reactivity towards
445 hydroxyl radicals as electrophilic species is lower the more nitro groups are present in the
446 molecule. Amino groups have the opposite effect and increase the π-electron density, thus
447 enhancing reactivity towards OH-radical attack. Interestingly, it was observed that NACs with two
448 *ortho*-methyl nitro substituents are less reactive than their isomers (2,4-DNT > 2,6-DNT and 2-
449 ADNT > 4-ADNT). When investigating the UV-promoted Fenton oxidation of NACs, Li *et al.*[45] also
450 found that the reaction rate decreases in the order 2-NT > 4-NT > 2,4-DNT > 2,6-DNT > TNT and
451 found a correlation with the charge density on the benzylic C-H-bonds. The authors attributed
452 their observations on the one hand to decreased resonance stabilization of *ortho* nitro
453 compounds and thus higher susceptibility to OH• attacks, as *ortho* nitro groups are forced out of
454 the ring plane, and on the other hand to steric shielding of the methyl group from radical attack.[48]
455 Therefore, NACs with nitro groups in *ortho* position to the methyl group are not only degraded
456 in a less favourable way when adsorbed to FeFAU55, but also when freely dissolved. Absence of
457 the methyl group decelerates the reaction of nitrobenzenes (NB, DNB, and TNB), but has an
458 accelerating effect for aminonitrobenzenes (DNA and DANB) compared to the respective
459 toluenes. It was already suspected by Liou *et al.*[20] that the methyl group is the preferred site of
460 radical attack for electron-deficient toluenes, which is a possible reason for NTs, DNTs, and TNT
461 to react faster than NB, DNB, and TNB.[20] For aminonitro compounds, radical attack to the methyl
462 group appears to be less preferred due to enhanced electron density in the aromatic ring.

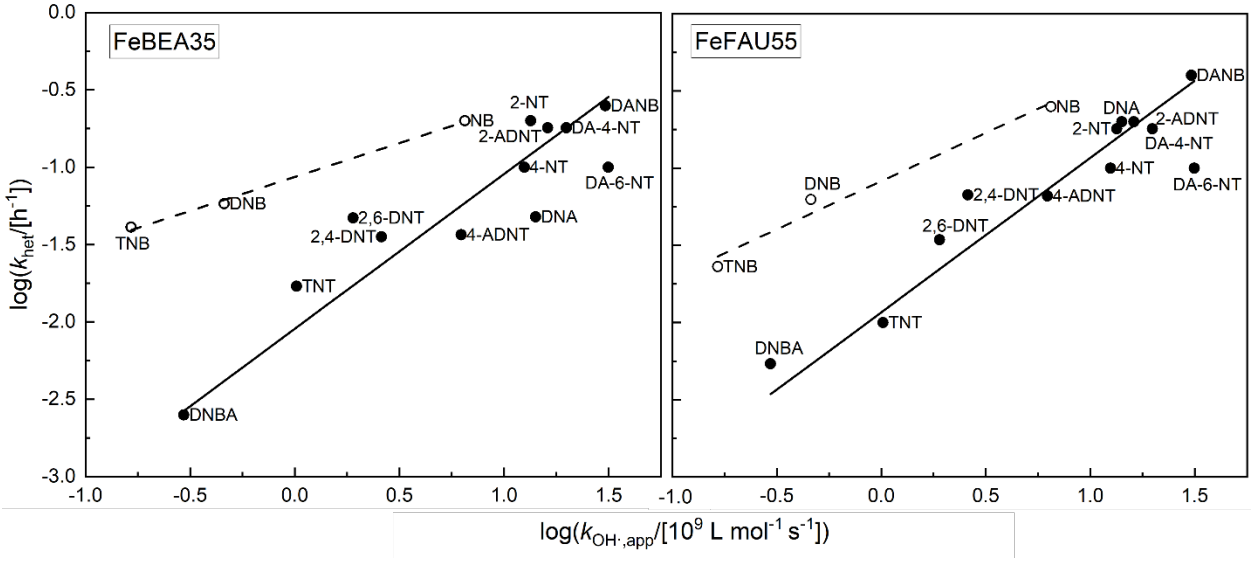

Figure 6: Double-logarithmic plots of the reaction rate constants of NAC degradation in the heterogeneous, Fenton-like Trap-Ox system k_{het} using FeBEA35 (left) and FeFAU55 (right) vs. the respective apparent second-order rate constant $k_{OH\cdot,app}$ of the homogeneous, stoichiometric Fenton reaction (for more details see Table 5 and section SI-3).

In the next step, the heterogeneous and homogeneous reaction rate constants were related to gain insight into the role of sorption in the reaction mechanism. In Figure 6, the double-logarithmic plots of the k_{het} vs. the $k_{OH\cdot,app}$ values are shown. The solid correlation lines between k_{het} and $k_{OH\cdot,app}$ implemented in Figure 6 are lines with the slope of 1. This slope implies that the selectivity of the oxidation is the same in both the heterogeneous and the homogeneous systems. Thus, adsorption in the zeolite does not play a significant role in substrate selectivity. Along this line, a reaction mechanism in which free OH-radicals are generated at the Fe-centres, which then attack the physisorbed NACs, is plausible. Thus, adsorption in the zeolite causes only an enrichment of the substrate molecules. Since this is the same for all substrates, as in the present case (equal loadings q), adsorption does not appear to interfere with the reaction mechanism.

The nitrobenzenes do not follow this correlation in both zeolites. This observation is conclusive in that the nitrobenzenes, unlike the nitrotoluenes, do not have a methyl group as a preferred site of initial radical attack. However, the amino-nitrobenzenes with no methyl group as well, fit the correlation. Moreover, the missing methyl groups can hardly explain the increased reactivity of nitrobenzenes compared to nitrotoluenes in the adsorbed state. In conclusion, we do see significant correlations between reaction selectivities in homogeneous and heterogeneous oxidation of NACs. However, they are not interpretable straightforwardly. It should be noted that some curved instead of straight lines obtained in the double-logarithmic plots (log (c/c_0) shown in Figure SI-5) indicate complex reaction kinetics during the determination of the $k_{OH\cdot,app}$-values (for example due to superimposition of stoichiometric and catalytic Fenton reactions or reactions

488 with other radical species than OH•). However, the $k_{OH\cdot,app}$-values of all nitrobenzenes would
489 have to be higher by a factor of 10 to fit the correlation obtained for the other NACs. A
490 mechanistic background of the increased reactivity of the nitrobenzenes in the heterogeneous
491 system can therefore be assumed. This observation again indicates that the presence of a methyl
492 group plays a role for the sorption of nitrotoluenes, especially on FeFAU55. Stronger specific
493 adsorption on the downside decreases the reactivity of adsorbed NACs.

494 On the other hand, there is also clear evidence in our results for the essential role of adsorption
495 in the zeolite-based oxidation of NACs: under the given experimental conditions, DNBA is
496 predominantly present as anion (pK_a = 1.4)[35]. The comparison with dinitrobenzene shows that
497 both compounds react with similar rates in the homogeneous system (DNBA: $k_{OH\cdot,app} = 0.3 \cdot 10^9$
498 L mol^{-1} s^{-1} vs. DNB: $k_{OH\cdot,app} = 0.5 \cdot 10^9$ L mol^{-1} s^{-1}). However, in the heterogeneous Trap-Ox system,
499 the rate constant of DNB is ten times higher than that of DNBA (DNB: k_{het} = 0.06 h^{-1} on both
500 zeolites vs. DNBA: k_{het} = 0.003 h^{-1} on FeBEA35 and 0.005 h^{-1} on FeFAU55). This is in line with a
501 large fraction of freely dissolved DNBA (≥ 90 %), which is not sufficiently close to the site of OH-
502 generation.

503 The reaction rate constants derived in this paragraph can be consulted to estimate which NACs
504 are preferentially degraded in Fenton-like reactions for mixed contaminations, as are usually
505 found at contaminated sites. In aged contaminations, where mainly amino derivatives of TNT are
506 present, TNT faces fast-reacting competitors and may be degraded itself in an unfavourable
507 manner due to its lower inherent reactivity. Furthermore, problems might arise because
508 dealkylated transformation products without amino groups also react slower than their parent
509 compounds, possibly leading to the release of nitrobenzenes (TNB, DNB, and NB, respectively).
510 Therefore, it is of utmost importance to ensure the further degradation of the slow-reacting
511 substances by sufficient contact with OH-radicals. Improved adsorption and thus retention within
512 the treatment zone as well as sufficiently high dosing of oxidant would be a way to achieve this.
513 The kinetic data for Trap-Ox oxidation presented in Figure 5 are promising with respect to the
514 unexpected high reactivity of nitrobenzenes.

515 **4. Conclusion and technological implication**

516 The adsorption and degradation of 15 nitroaromatic compounds (NACs) in the Trap-Ox Fe-zeolite
517 system, using the two Fe-loaded zeolites FeBEA35 and FeFAU55, was examined in this work. The
518 adsorption behaviour of the NACs varied significantly between the BEA-type and the FAU-type
519 zeolite. The adsorption to FeBEA35 could be described by regular L-type isotherms, reaching
520 maximum NACs loadings between 1.6 and 5.3 wt%. In contrast to that, the adsorption to
521 FeFAU55 was better described by S-type isotherms, with a very low slope at low loadings and a
522 steep increase in the medium part of the isotherm. This isotherm shape implies the existence of

523 a maximum adsorption coefficient $K_{D,max}$ (between $8.1 \cdot 10^4$ and $1.4 \cdot 10^6$ L kg^{-1} depending on the
524 individual NAC). Maximum loadings between 16 and 26 wt% were achieved.

525 The two zeolites showed similar catalytic activities for the NACs degradation. The oxidation of all
526 NACs in the Trap-Ox system could be observed by monitoring nitrate release as a helpful indicator
527 for the degradation progress. Nitrate yields of 50 to 100 % were achieved.

528 The rate constants derived from this nitrate release were related to apparent second order
529 reaction rate constants determined for the homogeneous Fenton reaction, which can be used to
530 estimate the intrinsic reactivity of the individual NACs in a Fenton-like reaction. Both rate
531 constants are lower for electron-deficient NACs with more nitro substituents, whereas amino
532 substituents accelerated the oxidation reaction. The correlation between both rate constants
533 indicates that the adsorption to the zeolites does not interfere deeply with the reaction
534 mechanism, where free OH-radicals generated at the Fe-centres attack the physisorbed NACs.
535 However, the nitrobenzenes examined in the frame of this work fall out of correlation, indicating
536 the presence of a mechanism increasing their reactivity in the adsorbed state compared to the
537 homogeneous system. Comparison of the hardly adsorbed 2,4-dinitrobenzoate with the well
538 adsorbed 1,3-dinitrobenzene proves the role of the adsorption as essential condition of catalytic
539 oxidation. Therefore, formation of intermediate products with a much lower adsorption affinity
540 and possibly lower reactivity to OH•, such as nitrated benzoic acids and ring-opened
541 nitroaliphatic compounds, may lead to a slower overall mineralization kinetics.

542 The results of this work open up an optimistic perspective for the application of Trap-Ox Fe-
543 zeolites for the adsorption and degradation of NACs also under groundwater conditions in the
544 field. In general, both Fe-zeolites are suitable for adsorption and degradation of NACs. The high
545 capacity of FeFAU55 allows for long lifetimes of an adsorptive barrier. However, as the
546 degradation of TNT proceeds significantly faster on FeBEA35, also mixed or consecutive barriers
547 are conceivable to combine fast TNT degradation while avoiding breakthrough of the early-stage
548 degradation product TNB. For TNT itself, the following scenario with an FeBEA35 barrier is
549 reasonable: 5 m barrier length with 0.5 wt% zeolite on aquifer sediment loading, a sediment true
550 density of 1.75 kg L^{-1} and porosity of 30 %, assuming a groundwater flow velocity of 0.5 m d^{-1} and
551 a $c_{TNT,input}$ = 0.2 mg L^{-1}. This would allow an operation time of more than 12 years until TNT
552 breakthrough. Common metabolites of TNT, such as 2-ADNT, would allow almost 23 years for
553 breakthrough.[10] After the contaminant retardation period, the permeable adsorption zone can
554 be regenerated by *in-situ* catalytic oxidation with H_2O_2.

555 A reasonable next step of this research following this perspective will be the consideration of
556 both adsorption and degradation in flow-through systems, as already demonstrated on the
557 example of MTBE.[12] Thereby, common models for the adsorption on FeBEA35 can be cross-
558 checked with experimental data, and new models for FeFAU55 should be developed. In addition,

559 further investigations should be accompanied by toxicological studies of the resulting reaction
560 products for the expected evidence that chemical degradation of the hazardous NACs is also
561 accompanied by an expected lowering of the hazard potential. Finally, the suitability of the
562 technology to remove NAC from groundwater should be validated in a pilot field test to
563 investigate the influence of site factors, e.g., natural organic matter or sediment composition.

564 **Declaration of Competing Interest**

565 The authors declare that they have no known competing financial interests or personal
566 relationships that could have appeared to influence the work reported in this paper.

567 **Acknowledgement**

568 The authors acknowledge the financial support received from the German Federal Ministry of
569 Education and Research (BMBF) in the frame of the project CONTASORB (grant number
570 03XP0090A). The project was supported by Intrapore GmbH from April 2018 to November 2019.

571 **Author Contributions**

572 The manuscript was written with contributions of all authors. All authors have given approval to
573 the final version of the manuscript.

574 **References**

575 (1) Köhler, J. *Explosivstoffe*, 10th ed.; Wiley - VCH, 2008. DOI: 10.1002/9783527623402.

576 (2) Lewis, T. A.; Newcombe, D. A.; Crawford, R. L. Bioremediation of soils contaminated with
577 explosives. *Journal of environmental management* **2004**, *70* (4), 291–307. DOI:
578 10.1016/j.jenvman.2003.12.005.

579 (3) Joos, A. *Natürliche Schadstoffminderung bei sprengstofftypischen Verbindungen*:*Feststellen,*
580 *Beurteilen, Nutzen*; DBU-LBEG-Tagung, 2009.

581 (4) Institute for Occupational Safety and Health of the German Social Accident Insurance.
582 *GESTIS substance database*. https://gestis-database.dguv.de/.

583 (5) Kovacic, P.; Somanathan, R. Nitroaromatic compounds: Environmental toxicity,
584 carcinogenicity, mutagenicity, therapy and mechanism. *Journal of Applied Toxicology* **2014**, *34*
585 (8), 810–824. DOI: 10.1002/jat.2980. Published Online: Feb. 16, 2014.

586 (6) Spain, J. C. Biodegradation of nitroaromatic compounds. *Annual review of microbiology*
587 **1995**, *49*, 523–555. DOI: 10.1146/annurev.mi.49.100195.002515.

588 (7) Bardos, P.; Merly, C.; Kvapil, P.; Koschitzky, H.-P. Status of nanoremediation and its
589 potential for future deployment: Risk-benefit and benchmarking appraisals. *Remediation*
590 *Journal* **2018**, *28* (3), 43–56. DOI: 10.1002/rem.21559.
591 (8) Corsi, I.; Winther-Nielsen, M.; Sethi, R.; Punta, C.; Della Torre, C.; Libralato, G.; Lofrano, G.;
592 Sabatini, L.; Aiello, M.; Fiordi, L.; Cinuzzi, F.; Caneschi, A.; Pellegrini, D.; Buttino, I. Ecofriendly
593 nanotechnologies and nanomaterials for environmental applications: Key issue and consensus
594 recommendations for sustainable and ecosafe nanoremediation. *Ecotoxicology &*
595 *Environmental Safety* **2018**, *154*, 237–244. DOI: 10.1016/j.ecoenv.2018.02.037. Published
596 Online: Feb. 22, 2018.
597 (9) Das, S. *Microbial biodegradation and bioremediation*; Elsevier Insights; Elsevier Science,
598 2014.
599 (10) Georgi, A.; Schierz, A.; Mackenzie, K.; Kopinke, F.-D. Colloidal activated carbon for in-situ
600 groundwater remediation - Transport characteristics and adsorption of organic compounds in
601 water-saturated sediment columns. *Journal of contaminant hydrology* **2015**, *179*, 76–88. DOI:
602 10.1016/j.jconhyd.2015.05.002. Published Online: Jun. 2, 2015.
603 (11) Gillies, G.; Raj, R.; Kopinke, F.-D.; Georgi, A. Suspension stability and mobility of Trap-Ox
604 Fe-zeolites for in-situ nanoremediation. *Journal of Colloid & Interface Science* **2017**, *501*, 311–
605 320. DOI: 10.1016/j.jcis.2017.04.037. Published Online: Apr. 12, 2017.
606 (12) Gonzalez-Olmos, R.; Kopinke, F.-D.; Mackenzie, K.; Georgi, A. Hydrophobic Fe-zeolites for
607 removal of MTBE from water by combination of adsorption and oxidation. *Environmental*
608 *Science & Technology* **2013**, *47* (5), 2353–2360. DOI: 10.1021/es303885y. Published Online: Feb.
609 14, 2013.
610 (13) Mackenzie, K.; Bleyl, S.; Kopinke, F.-D.; Doose, H.; Bruns, J. Carbo-Iron as improvement of
611 the nanoiron technology: From laboratory design to the field test. *The Science of the total*
612 *environment* **2016**, *563-564*, 641–648. DOI: 10.1016/j.scitotenv.2015.07.107. Published Online:
613 Aug. 20, 2015.
614 (14) Agrawal, A.; Tratnyek, P. G. Reduction of nitro aromatic compounds by zero-valent iron
615 metal. *Environmental Science & Technology* **1996**, *30* (1), 153–160. DOI: 10.1021/es950211h.

(15) Dodard, S. G.; Renoux, A. Y.; Hawari, J.; Ampleman, G.; Thiboutot, S.; Sunahara, G. I. Ecotoxicity characterization of dinitrotoluenes and some of their reduced metabolites. *Chemosphere* **1999**, *38* (9), 2071–2079. DOI: 10.1016/s0045-6535(98)00423-8.

(16) Held, T.; Draude, G.; Schmidt, F. R. J.; Brokamp, A.; Reis, K. H. Enhanced humification as an in-situ bioremediation technique for 2,4,6-trinitrotoluene (TNT) contaminated soils. *Environmental Technology* **1997**, *18* (5), 479–487. DOI: 10.1080/09593331808616563.

(17) Oh, S.-Y.; Yoon, H.-S.; Jeong, T.-Y.; Kim, S. D. Evaluation of remediation processes for explosive-contaminated soils: kinetics and Microtox ® bioassay. *Journal of Chemical Technology & Biotechnology* **2016**, *91* (4), 928–937. DOI: 10.1002/jctb.4658.

(18) Beltrán, F. J.; Encinar, J. M.; Alonso, M. A. Nitroaromatic hydrocarbon ozonation in water. 1. Single ozonation. *Industrial & Engineering Chemistry Research* **1998**, *37* (1), 25–31. DOI: 10.1021/ie9704253.

(19) Liou, M.-J.; Lu, M.-C. Catalytic degradation of nitroaromatic explosives with Fenton's reagent. *Journal of Molecular Catalysis A: Chemical* **2007**, *277* (1-2), 155–163. DOI: 10.1016/j.molcata.2007.07.030.

(20) Liou, M.-J.; Lu, M.-C.; Chen, J.-N. Oxidation of explosives by Fenton and photo-Fenton processes. *Water Research* **2003**, *37* (13), 3172–3179. DOI: 10.1016/S0043-1354(03)00158-1.

(21) Rodgers, J. D.; Bunce, N. J. Treatment methods for the remediation of nitroaromatic explosives. *Water Research* **2001**, *35* (9), 2101–2111. DOI: 10.1016/s0043-1354(00)00505-4.

(22) Schmelling, D. C.; Gray, K. A.; Kamat, P. V. Role of reduction in the photocatalytic degradation of TNT. *Environmental Science & Technology* **1996**, *30* (8), 2547–2555. DOI: 10.1021/es950896l.

(23) Li, X. D.; Schwartz, F. W. Permanganate oxidation schemes for the remediation of source zone DNAPLs and dissolved contaminant plumes. In *Chlorinated solvent and DNAPL remediation*; Henry, S. M., Warner, S. D., Eds.; ACS Symposium Series; American Chemical Society, 2002; pp 73–85. DOI: 10.1021/bk-2002-0837.ch005.

(24) Gonzalez-Olmos, R.; Holzer, F.; Kopinke, F.-D.; Georgi, A. Indications of the reactive species in a heterogeneous Fenton-like reaction using Fe-containing zeolites. *Applied Catalysis A: General* **2011**, *398* (1-2), 44–53. DOI: 10.1016/j.apcata.2011.03.005.

(25) Thomas, N.; Dionysiou, D. D.; Pillai, S. C. Heterogeneous Fenton catalysts: A review of recent advances. *Journal of Hazardous Materials* **2021**, *404* (124082). DOI: 10.1016/j.jhazmat.2020.124082.

(26) Esteve-Núñez, A.; Caballero, A.; Ramos, J. L. Biological degradation of 2,4,6-trinitrotoluene. *Microbiology and molecular biology reviews* **2001**, *65* (3), 335-52. DOI: 10.1128/MMBR.65.3.335-352.2001.

(27) Jiang, N.; Shang, R.; Heijman, S. G. J.; Rietveld, L. C. High-silica zeolites for adsorption of organic micro-pollutants in water treatment: A review. *Water Research* **2018**, *144*, 145–161. DOI: 10.1016/j.watres.2018.07.017. Published Online: Jul. 7, 2018.

(28) Qian, L.; Kopinke, F.-D.; Georgi, A. Photodegradation of perfluorooctanesulfonic acid on Fe-zeolites in water. *Environmental Science & Technology* **2021**, *55* (1), 614–622. DOI: 10.1021/acs.est.0c04558. Published Online: Dec. 17, 2020.

(29) Baerlocher, C.; McCusker, L. B. *Database of zeolite structures*. http://www.iza-structure.org/databases/.

(30) Gawel, A.; Seiwert, B.; Sühnholz, S.; Schmitt-Jansen, M.; Mackenzie, K. In-situ treatment of herbicide-contaminated groundwater - Feasibility study for the cases atrazine and bromacil using two novel nanoremediation-type materials. *Journal of Hazardous Materials* **2020**, *393*, 122470. DOI: 10.1016/j.jhazmat.2020.122470. Published Online: Mar. 5, 2020.

(31) García Einschlag, F. S.; Carlos, L.; Capparelli, A. L. Competition kinetics using the UV/H_2O_2 process: a structure reactivity correlation for the rate constants of hydroxyl radicals toward nitroaromatic compounds. *Chemosphere* **2003**, *53* (1), 1–7. DOI: 10.1016/S0045-6535(03)00388-6.

(32) Williams, M. A.; Rice, S. W. Wildlife toxicity assessment for 2-amino-4,6-dinitrotoluene and 4-amino-2,6-dinitrotoluene. In *Wildlife Toxicity Assessments for Chemicals of Military Concern*; Elsevier, 2015; pp 279–290. DOI: 10.1016/B978-0-12-800020-5.00016-8.

(33) Piccin, J. S.; Cadaval, T. R. S.; Pinto, L. A. A. de; Dotto, G. L. Adsorption Isotherms in Liquid Phase: Experimental, Modeling, and Interpretations. In *Adsorption Processes for Water Treatment and Purification*; Bonilla-Petriciolet, A., Mendoza-Castillo, D. I., Reynel-Ávila, H. E., Eds.; Springer International Publishing, 2017; pp 19–51. DOI: 10.1007/978-3-319-58136-1_2.

(34) Jiang, N.; Shang, R.; Heijman, S. G.; Rietveld, L. C. Adsorption of triclosan, trichlorophenol and phenol by high-silica zeolites: Adsorption efficiencies and mechanisms. *Separation and Purification Technology* **2020**, *235*, 116152. DOI: 10.1016/j.seppur.2019.116152.

(35) *CRC handbook of tables for organic compound identification*, 3. ed., 14. print; CRC Press, 1985.

(36) Lee, L. S.; Nyman, A. K.; Li, H.; Nyman, M. C.; Jafvert, C. Initial sorption of aromatic amines to surface soils. *Environmental Toxicology & Chemistry* **1997**, *16* (8), 1575–1582. DOI: 10.1002/etc.5620160803.

(37) Ainsworth, C. C. Transformation of 1-aminonapththalene at the surface of smectite clays. *Clays & Clay Minerals* **1991**, *39* (4), 416–427. DOI: 10.1346/CCMN.1991.0390411.

(38) Hauser, E. A.; Leggett, M. B. Color reactions between clays and amines. *Rubber Chemistry & Technology* **1940**, *13* (4), 942–947. DOI: 10.5254/1.3546573.

(39) Gao, M.; Fu, Q.; Wang, M.; Zhang, K.; Zeng, J.; Wang, L.; Xia, Z.; Gao, D. Facile synthesis of porous covalent organic frameworks for the effective extraction of nitroaromatic compounds from water samples. *Analytica chimica acta* **2019**, *1084*, 21–32. DOI: 10.1016/j.aca.2019.07.071. Published Online: Aug. 1, 2019.

(40) Haderlein, S. B.; Weissmahr, K. W.; Schwarzenbach, R. P. Specific adsorption of nitroaromatic explosives and pesticides to clay minerals. *Environmental Science & Technology* **1996**, *30* (2), 612–622. DOI: 10.1021/es9503701.

(41) Weissmahr, K. W.; Haderlein, S. B.; Schwarzenbach, R. P.; Hany, R.; Nüesch, R. In-situ spectroscopic investiations of adsorption mechanisms of nitroaromatic compounds at clay minerals. *Environmental Science & Technology* **1997** (31), 240–247. DOI: 10.1021/es960381+.

(42) Weissmahr, K. W.; Haderlein, S. B.; Schwarzenbach, R. P. Complex formation of soil minerals with nitroaromatic explosives and other π-acceptors. *Soil Science Society of America Journal* **1998**, *62* (2), 369. DOI: 10.2136/sssaj1998.03615995006200020012x.

(43) Gorb, L.; Gu, J.; Leszczynska, D.; Leszczynski, J. The interaction of nitrobenzene with the hydrate basal surface of montmorillonite: an ab initio study. *Physical Chemistry Chemical Physics* **2000**, *2* (21), 5007–5012. DOI: 10.1039/B004698L.

(44) Bish, D. L. Chapter 13.2 Parallels and distinctions between clay minerals and zeolites. In *Handbook of Clay Science 2006*; pp 1097–1112. DOI: 10.1016/S1572-4352(05)01040-8.

(45) Keiluweit, M.; Kleber, M. Molecular-level interactions in soils and sediments: the role of aromatic pi-systems. *Environmental Science & Technology* **2009**, *43* (10), 3421–3429. DOI: 10.1021/es8033044.

(46) Haderlein, S. B.; Schwarzenbach, R. P. Adsorption of substituted nitrobenzenes and nitrophenols to mineral surfaces. *Environmental Science & Technology* **1993**, *27* (2), 316–326. DOI: 10.1021/es00039a012.

(47) Weissmahr, K. W.; Hildenbrand, M.; Schwarzenbach, R. P.; Haderlein, S. B. Laboratory and field scale evaluation of geochemical controls on groundwater transport of nitroaromatic ammunition residues. *Environmental Science & Technology* **1999**, *33* (15), 2593–2600. DOI: 10.1021/es981107d.

(48) Li, Z. M.; Shea, P. J.; Comfort, S. D. Nitrotoluene destruction by UV-catalyzed fenton oxidation. *Chemosphere* **1998**, *36* (8), 1849–1865. DOI: 10.1016/s0045-6535(97)10073-x.

(49) Sviatenko, L. K.; Gorb, L.; Hill, F. C.; Leszczynska, D.; Leszczynski, J. Structure and redox properties of 5-amino-3-nitro-1H-1,2,4-triazole (ANTA) adsorbed on a silica surface: A DFT M05 computational study. *The Journal of Physical Chemistry A* **2015**, *119* (29), 8139–8145. DOI: 10.1021/acs.jpca.5b03393. Published Online: Jul. 9, 2015.

(50) Fukushima, M.; Tatsumi, K.; Morimoto, K. The Fate of Aniline after a Photo-Fenton Reaction in an Aqueous System Containing Iron(III), Humic Acid, and Hydrogen Peroxide. *Environmental Science & Technology* **2000**, *34* (10), 2006–2013. DOI: 10.1021/es991058k.

(51) Liou, M.-J.; Lu, M.-C.; Chen, J.-N. Oxidation of TNT by photo-Fenton process. *Chemosphere* **2004**, *57* (9), 1107–1114. DOI: 10.1016/j.chemosphere.2004.07.053.

(52) Ayoub, K.; Nélieu, S.; van Hullebusch, E. D.; Maia-Grondard, A.; Cassir, M.; Bermond, A. TNT oxidation by Fenton reaction: Reagent ratio effect on kinetics and early stage degradation pathways. *Chemical Engineering Journal* **2011**, *173* (2), 309–317. DOI: 10.1016/j.cej.2011.07.022.

(53) García Einschlag, F. S.; Lopez, J.; Carlos, L.; Capparelli, A. L.; Braun, A. M.; Oliveros, E. Evaluation of the efficiency of photodegradation of nitroaromatics applying the UV/H2O2

technique. *Environmental Science & Technology* **2002**, *36* (18), 3936–3944. DOI: 10.1021/es0103039.

(54) Ho, P. C. Photooxidation of 2,4-dinitrotoluene in aqueous solution in the presence of hydrogen peroxide. *Environmental Science & Technology* **1986**, *20* (3), 260–267. DOI: 10.1021/es00145a007.

(55) Tanaka, K.; Luesaiwong, W.; Hisanaga, T. Photocatalytic degradation of mono-, di- and trinitrophenol in aqueous TiO_2 suspension. *Journal of Molecular Catalysis A: Chemical* **1997**, *122* (1), 67–74. DOI: 10.1016/S1381-1169(96)00509-2.

(56) Grätzel, C. K.; Jirousek, M.; Grätzel, M. Decomposition of organophosphorus compounds on photoactivated TiO_2 surfaces. *Journal of Molecular Catalysis* **1990**, *60* (3), 375–387. DOI: 10.1016/0304-5102(90)85260-O.

(57) Oh, S.-Y.; Chiu, P. C.; Kim, B. J.; Cha, D. K. Enhancing Fenton oxidation of TNT and RDX through pretreatment with zero-valent iron. *Water Research* **2003**, *37* (17), 4275–4283. DOI: 10.1016/S0043-1354(03)00343-9.